Available online at www.sciencedirect.com
ScienceDirect
Chaos, Solitons and Fractals 32 (2007) 711–724
CHAOS
SOLITONS & FRACTALS
www.elsevier.com/locate/chaos

Basins of attraction of nonlinear wave–wave interactions

José C.P. Coninck, Sergio R. Lopes, Ricardo L. Viana *

Departamento de Física, Universidade Federal do Paraná, Caixa Postal 19081, 81531-990 Curitiba, Paraná, Brazil

Accepted 8 November 2005

Communicated by Prof. J. Kapitaniak

Abstract

The nonlinear interaction of two wave triplets, with a non-zero frequency mismatch, has been found to present many indications of complex behavior. Considering the presence of dissipation, there are coexistent periodic and chaotic attractors in the high-dimensional phase space of the system. Their basin structure is also complex, parts of it being densely mixed in arbitrarily fine scales. We claim that the fractal part of the basin boundary presents the so-called Wada property, for which points on the boundary are arbitrarily close to points of all coexisting basins. The practical consequence of this fact is that, given a small yet non-zero uncertainty on determining the initial condition, the asymptotic state to which the system goes is almost completely uncertain.

1. Introduction

Parametric interactions of three and four waves are modelled by systems of coupled-mode nonlinear differential equations whose solutions are found to exhibit a wide variety of dynamical phenomena, from periodic to chaotic behavior, being also one of the oldest physical applications of nonlinear dynamics and chaos [1,2]. Nonlinear wave–wave interactions occur in many physical examples, mainly in plasma physics and optics. Some of these applications are anomalous laser absorption and laser beam filamentation in laboratory plasmas [3], auroral radio emissions [4], solar wind modulation [5], second-harmonic production and handling of optical signals [6], wave mixing in chiral liquids [7], generation of soft X-rays by conversion of visible laser [8] and production of Raman waves (lasers) using dielectric micro-cavity [9]. Coherent four-wave interactions appear also in nonlinear atom optics (interacting Bose-Einstein condensates) [10]. Parametric wave interaction plays an important role in laser physics (conversion of incoherent light into coherent light) [11,12].

The conservative version of the four-wave interaction (for the model treated in this paper), when the wave frequencies match exactly each other, is integrable in the Liouville sense, and analytical integrals of motion are known [13]. If there is a frequency mismatch, however, the system loses integrability and complex dynamics can occur, including periodic, quasi-periodic, and chaotic motion in a high-dimensional phase space [14,15]. When dissipation is added to the

* Corresponding author.

0960-0779/$ - see front matter
doi:10.1016/j.chaos.2005.11.061

four-wave interaction, there are many qualitative changes in the system dynamics. The absence of an energy surface in the phase space leads to the appearance of attracting and repelling sets, either periodic or chaotic. The number of coexisting attractors in the system has been found to increase in a power-law fashion with decreasing relative triplet frequency mismatch [16]. Hence, the phase space of the system typically displays multi-stable behavior, and the ultimate behavior of the trajectories depends on the initial condition chosen.

These coexisting attractors, on the other hand, have their own basins of attraction, with a complex structure expected for such dynamical systems [17]. For some values of the dissipation parameters, we have found an invariant manifold, embedded in the phase space of the system, to which the phase trajectories are attracted for large times [18]. The dynamics on this manifold is conservative, since it preserves an energy-like constant as time evolves; and the dissipative effects are found in the directions transversal to this invariant manifold.

The purpose of this paper is to investigate some properties of the basin structure characteristic of the dissipative four-wave interaction system. Our first observation was that the boundary between basins of different attractors has fractal properties. Hence the basins are tightly interwoven along phase space regions, particularly near to an unstable orbit at the origin. However, we cannot assert that the basin boundary is intertwined in arbitrarily fine scales, in the sense described in Ref. [19] for the kicked double rotor map, where for any phase space region (no matter how small) for which the boundary has a fractal nature, one can choose subregions within it for which the boundary is a smooth surface.

The basin boundary structure we found presents a close resemblance with the so-called riddled basins, for which at least one of the basins of attraction has the property that any neighborhood about each point within that basin contains points belonging to another basin [20]. If all basins of attraction are riddled, they are called intermingled basins, which have been described in high-dimensional dynamical systems like lattices of coupled maps and oscillator, but they can appear in lower-dimensional models as well [21]. In higher-dimensional dynamical systems of physical interest it is usually difficult to verify the strict mathematical conditions under which one or more basins are riddled. The idea of *practical riddling* has been introduced to cope with such situations [22].

The observable consequence of such extremely convoluted aspect of the boundary between basins of attraction is that it becomes virtually impossible to know a priori to what attractor will a given initial condition asymptote to. Fractal basin boundaries present a milder version of this effect, called *final state sensitivity*, for which even a dramatic improvement in the precision to which an initial condition is determined in phase space does not improve much the uncertainty about to what attractor the system will asymptote to [23,24]. Fractal basin boundaries with a box-counting dimension close to the phase-space dimension itself are related to an extreme form of this effect, rendering practically innocuous—from the point of view of final state prediction—any efforts on improving the precision of the initial condition determination.

Related to this observable effect, we found that the fractal basin structure possess the so-called Wada topological property. A basin boundary possessing the Wada property is such that any point which is on the boundary of one basin is also simultaneously on the boundary of all the other basins [25,26]. The Wada property has been extensively investigated in dissipative systems like the Hénon map [25]; and in systems of practical interest, like the three-disk billiard [27], the scattering by a Hénon-Heiles potential [28], light scattering by reflecting spheres [29], quasi-periodically driven system [17], the advection of tracers in fluid flows [30], and magnetic field line escape in fusion machines [31]. Due to the large dimensionality of the phase space, we have to resort mainly on numerical diagnostics to prove the above claims. However, since a complex basin structure has been found to be typical of high-dimensional systems, this is likely to be the case also in the wave–wave interactions.

The rest of the paper is organized as follows: in Section 2 we present the basic equations of the four-wave interaction model. Section 3 shows the structure of the basins of attractions for bounded and unbounded attractors observed for a given set of parameter values, and explore their extreme sensitivity to the final state. The relative importance of unbounded attractors, and its relation with the system dynamics is commented on in Section 4. Section 5 is devoted to a numerical verification of the Wada property in the basin structure. Our conclusions are left to the final section.

2. Resonant four-wave interaction

We study a particular kind of wave–wave interaction namely, the nonlinear interaction of four waves, with two of them participating simultaneously in two resonant triplets, such that we have four waves in total. This system, in its conservative regime, was first studied by Sugihara [32] and Karplyuk and coworkers [33], who have derived some particular solutions for the coupling, considering the case of perfect matching conditions among the waves involved. The integrability of this particular form of the conservative interaction of the four-wave coupling, for the case of perfect frequency mismatches, was proved by Romeiras [13]. When there are imperfect frequency matching conditions, the

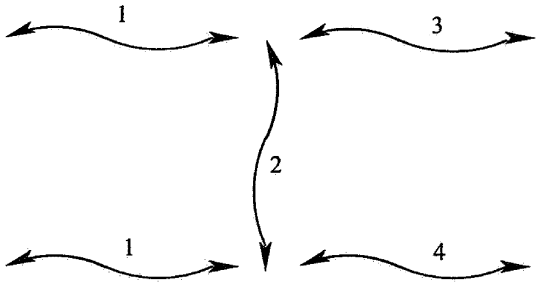

Fig. 1. Scheme of the four-wave interaction.

four-wave interaction consists of a two degree-of-freedom Hamiltonian problem, and thus presents regular and chaotic orbits, depending on the particular initial condition given for the interaction [15].

The simplest mathematical model for describing the temporal dynamics of a resonant nonlinear coupling of four waves can be obtained by assuming that the nonlinearity is sufficiently weak, such that only quadratic terms in the wave amplitudes need to be considered. Moreover, we assume monochromatic waves whose electric fields can be written in the modulational form $E_\alpha(\mathbf{x},t) = (1/2)A_\alpha(\mathbf{x},t)\exp \mathrm{i}(\mathbf{k}_\alpha \cdot \mathbf{x} - \omega_\alpha t) + \text{c.c.}$ (where $\alpha = 1,2,3,4$).

The resonant four-wave parametric interaction considered in this paper is comprised by the nonlinear coupling of two three-wave sets (triplets), with the following phase-matching conditions (a schematic representation of this coupling is depicted in Fig. 1):

$$\omega_3 = \omega_1 - \omega_2 \pm \delta_3, \tag{1}$$

$$\omega_4 = \omega_1 + \omega_2 \pm \delta_4, \tag{2}$$

$$\mathbf{k}_3 = \mathbf{k}_1 - \mathbf{k}_2, \tag{3}$$

$$\mathbf{k}_4 = \mathbf{k}_1 + \mathbf{k}_2, \tag{4}$$

where $\delta_{3,4}$ are the frequency mismatches for each of the wave triplets.

Making use of the first and second momenta of the Boltzmann equation (continuity and motion equation, respectively), with the Lorentz force term, and with help of Maxwell equations and the linear dispersion relation $\omega_\alpha(\mathbf{k}_\alpha)$ of each interacting wave, it is possible to derive second-order differential equations for the wave field amplitude. This set of equations can be further simplified by considering that the nonlinearities are weak enough, such that the timescale of the nonlinear interactions between the wave triplets is much longer than the periods of the linear (uncoupled) waves, what amounts to the condition $\omega^{-1} \ll A(\partial_t A)^{-1}$. Proceeding in this way, there can be obtained a set of four first-order coupled differential equations describing the four-wave interaction problem. The details of the derivation can be found in Ref. [34].

In the following we adopt the modulational notation for the wave fields: $\mathbf{E}_\alpha(\mathbf{x},t) = \frac{1}{2}A_\alpha(t)\exp[\mathrm{i}(\mathbf{k}_\alpha \cdot \mathbf{x} - \omega_\alpha t)] + \text{c.c.}$, where we are considering that $A_\alpha(t)$ is a spatially homogeneous and slowly varying complex envelope, which can be further represented in the form

$$A_\alpha(t) = \mathrm{Re}(A_\alpha) + \mathrm{i}\,\mathrm{Im}(A_\alpha) = |A_\alpha|\mathrm{e}^{\mathrm{i}\phi_\alpha} \quad (\alpha = 1,2,3,4). \tag{5}$$

In terms of these normalized complex amplitudes, the equations of the resonant parametric four-wave coupling are

$$\frac{\mathrm{d}A_1}{\mathrm{d}t} = A_2A_3 - rA_2^*A_4 + v_1A_1, \tag{6}$$

$$\frac{\mathrm{d}A_2}{\mathrm{d}t} = -A_1A_3^* - rA_1^*A_4 + v_2A_2, \tag{7}$$

$$\frac{\mathrm{d}A_3}{\mathrm{d}t} = -A_1A_2^* + \mathrm{i}\delta_3A_3 + v_3A_3, \tag{8}$$

$$\frac{\mathrm{d}A_4}{\mathrm{d}t} = rA_1A_2 - \mathrm{i}\delta_4A_4 + v_4A_4, \tag{9}$$

where $\delta_3 > 0$ and $\delta_4 > 0$ are the normalized linear frequency mismatches, $0 < r < 1$ is the coupling parameter between triplets, $v_1 > 0$ is the linear energy injection coefficient, and $v_2 < 0$, $v_3 < 0$, and $v_4 < 0$ are dissipation parameters.

Since each wave field is characterized by two real parameters (amplitude $|A_\alpha|$ and phase ϕ_α), they are out of eight dynamical variables in this system, whose phase space is accordingly eight-dimensional. This number can be further decreased, by two units, by using the phase conjugacies given by the Stokes and anti-Stokes modes

$$\phi_+ = \phi_1 + \phi_2 - \phi_4, \tag{10}$$

$$\phi_- = \phi_1 - \phi_2 - \phi_3 \tag{11}$$

and the system dynamics is constrained to a six-dimensional subset of the phase space, even when the dissipation coefficients v_i have non-zero values.

Since the vector field we dealt with is holomorphic in the complex phase space [35], the time rate of phase space volume change can be evaluated by the divergence of the real and imaginary parts of the complex vector field described by Eqs. (6)–(9):

$$\mathscr{J} = \sum_{i=1}^{4} \frac{\partial \mathrm{Re}\{\dot{A}_i\}}{\partial \mathrm{Re}\{\dot{A}_i\}} + \frac{\partial \mathrm{Im}\{\dot{A}_i\}}{\partial \mathrm{Im}\{\dot{A}_i\}} = 2\sum_{i=1}^{4} v_i \tag{12}$$

resulting in a constant value, in such a way that the system is globally dissipative (anti-dissipative), i.e., the volumes shrink (expand) with time at the same rate everywhere in the available regions of the phase space. In the following, we will set $v_1 = 1.0$, $v_2 = v_3 = v_4 = -0.8$, and $r = 1.0$; such that $\mathscr{J} < 0$. We also define a symmetry-breaking parameter

$$\Delta = \delta_3 - \delta_4, \tag{13}$$

which measures the total mismatch between triplets. The physical interpretation of δ_3 and δ_4 parameters is that they measure how efficient is the energy transport from one wave to another, interacting in each wave triplet, such that Δ can be understood as how different is the energy flux in each triplet. If $\Delta = 0$ both triplets are indistinguishable.

3. Extreme final sensitivity

We will analyze the system dynamics using the symmetry-breaking Δ as a tunable control parameter. The dynamics in the phase space of the dissipative and non-symmetric wave–wave interaction will be described, in what follows, by the real and imaginary parts of the field amplitudes A_i. We will choose to work with a two-dimensional projection in the $\mathrm{Re}(A_1)$–$\mathrm{Im}(A_1)$ plane.

Fig. 2 depicts such a projection for $\Delta = 0.01$ and $r = 1.0$, in which there are just two different coexisting attractors, which are limit cycles named as $P1$ [Fig. 2(a)] and $P3$ [Fig. 2(b)]. The notation follows from a Poincaré one-dimensional section on this surface, consisting of the positive half of the vertical axis, starting at the origin (0,0). The PI (P3) cycle

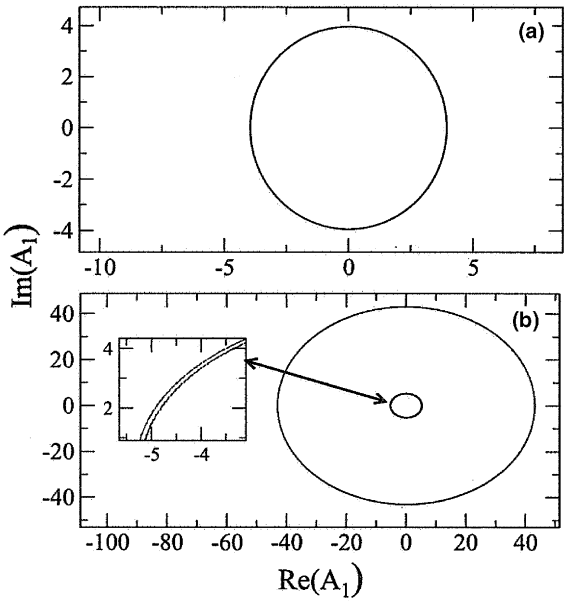

Fig. 2. Periodic attractors, in a $\mathrm{Re}(A_1)$–$\mathrm{Im}(A_1)$ projection of the phase space for the four-wave dissipative system with $\Delta = 0.01$ and $r = 1.0$. The units shown in the axes are arbitrary, (a) $P1$ limit cycle; (b) $P3$ limit cycle (see inset for a magnification showing in detail the inner band).

corresponds to a stable period-1 (3) orbit at this section (in the latter case, there are two inner curves extremely close to each other but distinguishable in the magnification shown in Fig. 2(b) inset). Moreover, there is an attractor at infinity, corresponding to effectively uncoupled waves, and the amplitude of one wave increases indefinitely with time. We interpret the attractor at infinity as a consequence of the waves being uncoupled, up to the nonlinear terms kept in the physical model (in our case, the quadratic terms). If these higher-order terms were included in the model, the attractor at infinity would be replaced by a bounded attractor, reflecting a saturation of large, amplitude waves due to higher-order terms.

Although these are periodic attractors, their basins turn out to be highly interwoven, as shown by Fig. 3(a), which shows another projection of the phase space ($\mathrm{Re}(A_1)$–$\mathrm{Re}(A_3)$) for the same parameters used in Fig. 2, for which $\Delta = 0.01$. The basin of the $P1(P3)$ is colored in gray (white), whereas the basin of the attractor at infinity is depicted in black.

These three basins are mixed together in a complicated way. To show that this is not merely an artifact of the special projection used, in Fig. 3(b)–(d) we depict the same basins of attraction in different projections, namely $\mathrm{Re}(A_1)$–$\mathrm{Im}(A_1)$, $\mathrm{Re}(A_4)$–$\mathrm{Im}(A_3)$, and $\mathrm{Re}(A_2)$–$\mathrm{Im}(A_2)$.

The projections shown by Fig. 3 strongly suggest that at least a portion of the basins of the periodic attractors $P1$ and $P3$ as well as of the attractor at infinity are highly interwoven in a portion of the system phase space, so indicating a fractal basin boundary between them. A well-known consequence of the presence of fractal basin boundaries is final state sensitivity [23]. Any initial condition is known up to a given uncertainty ϵ, such that we can think of a hyper-sphere of radius ϵ centered at that initial condition in the phase space. If the initial condition is so near the fractal boundary that the ϵ-sphere intercepts the basin boundary, we cannot be sure if that initial condition will evolve to one or another

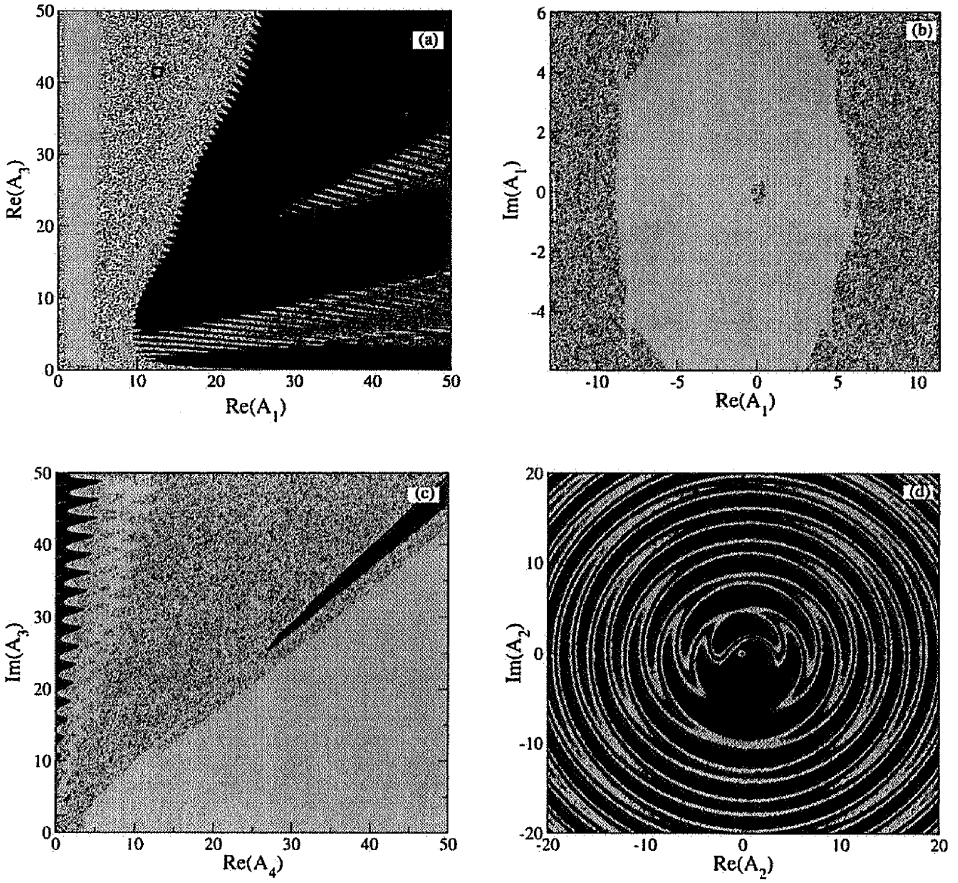

Fig. 3. Projections of the phase space of the four-wave interaction system with $\Delta = 0.01$, $r = 1.0$, and showing the basins of attraction of the bounded attractors $P1$ (gray), $P3$ (white) and the infinity (black). The projection axes are: (a) $\mathrm{Re}(A_1)$–$\mathrm{Re}(A_3)$; (b) $\mathrm{Re}(A_1)$–$\mathrm{Im}(A_1)$; (c) $\mathrm{Re}(A_4)$–$\mathrm{Im}(A_3)$ (d) $\mathrm{Re}(A_2)$–$\mathrm{Im}(A_2)$.

basin or else will diverge to infinity. The union of all ϵ-spheres intercepting the basin boundary yields the uncertain fraction (after dividing by the area of the phase space region to be analyzed) $F(\epsilon)$.

For fractal basin boundaries, the uncertain fraction scales in a power-law fashion with the uncertainty ball radius: $F(\epsilon) \sim \epsilon^{\alpha}$, where α is the so-called *uncertainty exponent*. If d is the box-counting boundary dimension, it follows that $\alpha = D - d$ [24], where D is the phase space dimension. The more involved the basin boundary is, the higher is its box-counting dimension (i.e. closer to the phase plane dimension D). Hence, d can be used as a rough measure of the complexity of the basin structure.

We selected a region comprised a representative portion of the basin boundaries (the small box in the upper-left corner in Fig. 3(a)) and covered it with a fine mesh of initial conditions. At each initial condition **A** we choose at random another initial condition **B** inside an ϵ-sphere centered at **A**. If **A** and **B** lead to orbits asymptoting to different attractors (or escaping out to infinity) we then call **A** a ϵ-uncertain initial condition. The uncertain fraction was estimated from the ratio between the number of all uncertain conditions and the total number of initial conditions (the number of mesh points).

The uncertainty exponent was obtained from a least-squares fit in a log–log plot of $F(\epsilon)$ versus ϵ, our results being depicted in Fig. 4. We used 5000 initial conditions for each point, with a correlation coefficient of 0.9180 and regression coefficient 0.0222. Our results point out to a value of the uncertainty exponent α near zero, which indicates an extremely intertwined basin structure. Let us explore some consequences of this result. In numerical simulation of system trajectories in phase space, ϵ can be regarded as the precision with which an initial condition is specified, such that the uncertainty exponent α gives the probability $\mathscr{P}(\epsilon)$ that the numerically determined asymptotic behavior accurately reflects the true dynamics of the system [21]. If α is less than unity in general, even a drastic decreasing of ϵ will result in a modest reduction of $\mathscr{P}(\epsilon)$. In the limiting case when $\alpha \approx 0$, even an improvement of many orders of magnitude in the precision with which the initial condition is specified will result in practically no improvement in our ability to forecast the asymptotic state of the system in a reliable way. This has been called *extreme final sensitivity* [21].

This result was obtained for a symmetry-breaking parameter value of $\Delta = 0.01$, but it persists over many orders of magnitude, as can be observed in Fig. 5, where the uncertainty exponent is plotted versus Δ. For all Δ-values used we considered a small box near to the fixed point at the origin (the rectangle $-0.250 < x < 0.250$, $-3 < y < 3$) and used out of 600 initial conditions for 6 different values of ϵ, from 10^{0} to 10^{-5}. The uncertainty exponent $\alpha = 0.022$ remains nearly constant even when Δ is varied over five decades, with a correlation coefficient 0.98 ± 0.03. This suggests that the extreme final sensitivity observed in the basin structure is not noticeably affected by symmetry-breaking, as long as Δ is non-zero (for the $\Delta = 0$ case see Ref. [15]), being rather a robust manifestation of the underlying dynamics of the four-wave interaction. Moreover, the basin boundary dimension embedded in the two-dimensional phase space projection is $d = 2 - \alpha = 1.977$, thus making for an almost area-filling curve.

In order to illustrate the significance of this value of α in terms of our ability to forecast the asymptotic behavior of the four-wave system, let us assume that the value of the uncertainty radius ϵ can be specified to within 10^{-16},

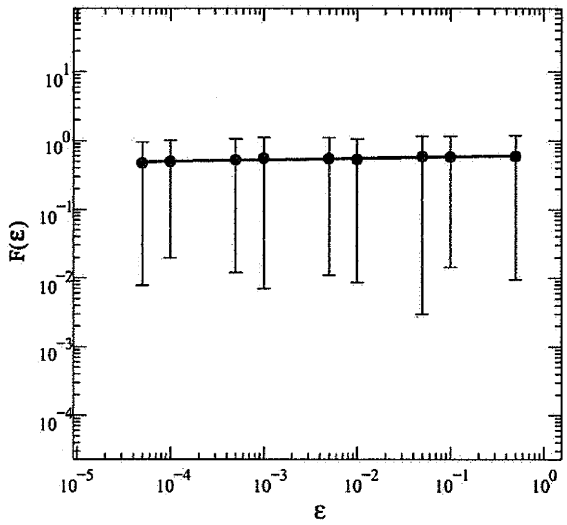

Fig. 4. Uncertain fraction of initial conditions versus the uncertainty radius ϵ for a box picked up from Fig. 3(a) near the point with coordinates (13,42).

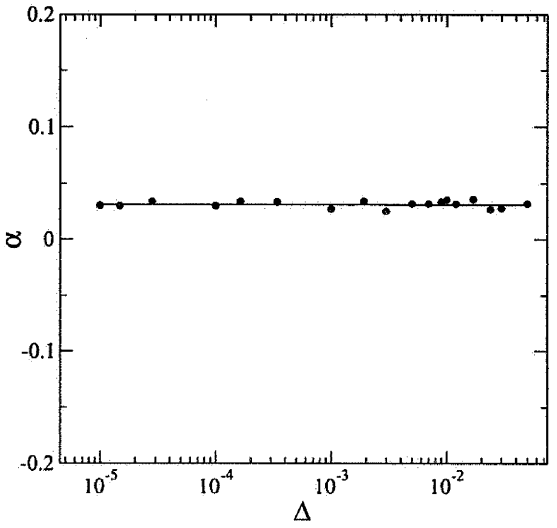

Fig. 5. Uncertainty exponent as a function of the symmetry-breaking parameter, for five orders of magnitude.

i.e., the standard truncation limit of double precision floating-point numbers. Then there is a probability of $\mathscr{P}(10^{-16}) \sim 10^{0.022\times(-16)} \sim 0.44$ that the final asymptotic state (either $P1$, $P3$ or infinity) has been wrongly determined by numerical computations. Even a substantial improvement in the precision with which the initial conditions are determined (by using quadruple precision, for example) is insufficient to yield more than a tiny improvement in the decreasing of the probability of getting an incorrect final state. Hence, some computer calculations of the asymptotic state of the four-wave system cannot in fact be utterly reliable.

4. Bounded and unbounded attractors

The structure of the basins of attraction depends on the underlying dynamics of the vector field (6)–(9), even though many of the features are not amenable to an analytical approach due to the high-dimensionality of the phase space (which has out of eight dimensions). There is an equilibrium point at the origin $(A_i, A_i^*) = (0, 0)$ and which turns out to be locally unstable for the parameter ranges investigated in this work.

More specifically, on linearizing the vector field (6)–(9) at this equilibrium point, we obtain the following eigenvalues of the corresponding Jacobian matrix:

$$\xi_1 = \nu_1 > 0 \quad \xi_2 = \nu_1 > 0, \tag{14}$$

$$\xi_3 = \nu_2 < 0 \quad \xi_4 = \nu_2 < 0, \tag{15}$$

$$\xi_5 = \nu_3 + \mathrm{i}\delta_3 \quad \xi_6 = \nu_3 - \mathrm{i}\delta_3, \tag{16}$$

$$\xi_7 = \nu_4 + \mathrm{i}\delta_4 \quad \xi_8 = \nu_4 - \mathrm{i}\delta_4. \tag{17}$$

Since both ν_3 and ν_4 are negative, we have two positive real eigenvalues, corresponding to two unstable eigendirections which coincide with the $\mathrm{Re}(A_1)$ and $\mathrm{Im}(A_1)$ axes. Moreover, we have out of six eigenvalues with negative real parts, being two real and four complex conjugates, corresponding to a six-dimensional stable subspace.

The unstable directions emanating from the unstable fixed point at origin are closely related with the basin of the attractor at infinity. In fact, the latter physically represents a situation in which the first interacting wave (A_1) is effectively uncoupled with the other, such that a net energy injection would lead to a diverging behavior for the amplitude of this wave, represented by the attractor at infinity. On the other hand, the fixed point at origin is the unstable situation in which there are no interacting waves at all, and any wave perturbation of it tends to evolve according to the dissipative vector field (6)–(9). A bounded attractor, like those periodic orbits $P1$ and $P3$, represents a situation for which the energy injection on a given wave is counterbalanced by dissipation. If the dissipation is not strong enough to overcome energy injection, however, we may have a diverging behavior.

The relative size of the infinity basin of the attraction is influenced by the symmetry-breaking parameter, as can be appreciated in Fig. 6, where we depict in white the basins of both bounded attractors ($P1$ and $P3$) and, in black, the

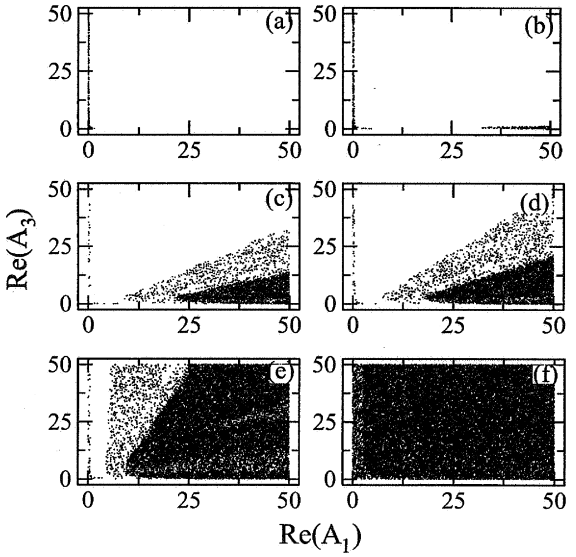

Fig. 6. Basins of attraction, in a Re(A_1)–Re(A_3) phase space projection, of the bounded (white pixels) and unbounded (black pixels) attractors for Δ = (a) 1.00×10^{-6}; (b) 2.00×10^{-4}; (c) 1.19×10^{-3}; (d) 2.30×10^{-3}; (e) 1.00×10^{-2}; (f) 4.00×10^{-1}.

basin of the attractor at infinity, in a Re(A_1)–Re(A_3) phase space projection. In the symmetric case ($\Delta = 0.0$) only the eigendirections Re(A_1) and Im(A_1) are unstable. For a small value of Δ (see Fig. 6(a)) we observed that the only "escape channel" to infinity is a thin line located at Re(A_1) = 0, which is a consequence of the unstable subspaces emanating from the fixed point at the origin.

Such result is entirely due to the limited power of the numerical integrator chosen (a 12th-order Adams predictor–corrector method), since the local divergence rate is too large and the numerical integration becomes rapidly unstable. As Δ increases [Fig. 6(b)] we observe a second escape channel whose projection is apparently orthogonal to the first channel, and also due to the unstable directions of the origin. For higher Δ [Fig. 6(c)–(e)] the basin of infinity develops over an increasing region of the phase space and, for Δ large enough [Fig. 6(f)] almost all points of the phase space region considered lead to an unbounded attractor.

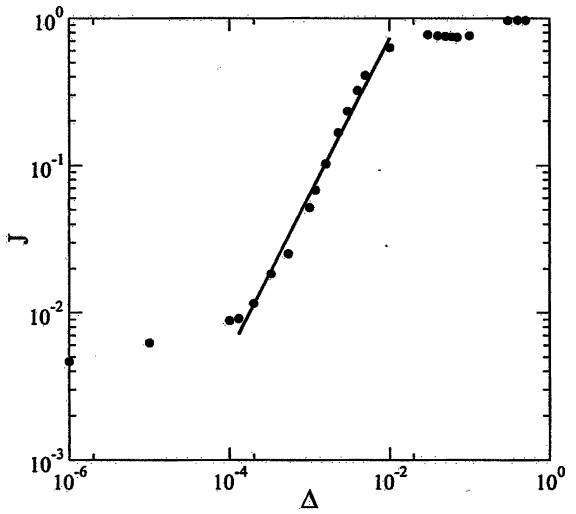

Fig. 7. Relative area of the basin of infinity as a function of the symmetry-breaking parameter.

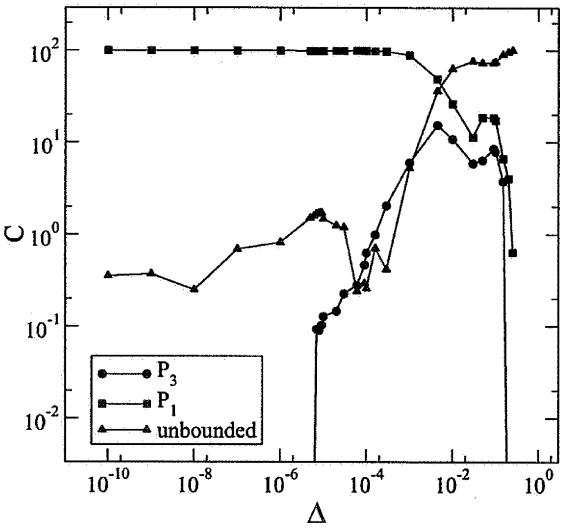

Fig. 8. Absolute area of the bounded and unbounded attractors as a function of the symmetry-breaking parameter.

The relative importance of the basin of the attractor at infinity can be measured by its relative area (J), with respect to the total area of the two-dimensional projection of the phase space region studied. The relative area of the basin of infinity is depicted in Fig. 7 as a function of the symmetry-breaking parameter. Each point results from the analysis of 40,000 initial conditions. As a general trend, the higher is the value of Δ, the more prevalent is the basin of infinity, as already suggested by Fig. 6. However, in the interval $10^{-4} < \Delta < 10^{-2}$ the increase scales as a power-law with an exponent 1.021 ± 0.04 (the correlation coefficient is 0.9918). For $\Delta \sim 1$, nearly all initial conditions asymptote to infinity. As the importance of the attractor of infinity grows with symmetry breaking, there is a decreasing of the basins of the bounded attractors. Likewise we compute the absolute area (C) of the basins of the bounded ($P1$ and $P3$) and unbounded attractors; our results being shown in Fig. 8, where the absolute areas C are plotted versus Δ. Each point in Fig. 8 results from out of 40,000 initial conditions.

For very small values of Δ the basin of $P1$ utterly dominates the phase space, with a tiny content of the infinity (unbounded attractor) basin. For $\Delta \approx 10^{-5}$ there emerges the basin of $P3$, which occupies a relative area which increases with Δ, and leading to a weaker dominance of the $P1$ basin. This indicates that the basin of $P3$ is born within the basin of $P1$, a result which actually comes from the hierarchy of the orbits [36]. As Δ approaches unity, both $P1$ and $P3$ lose relative importance to the basin of infinity, which dominates the phase space in this limit.

5. Wada basins

There is an interesting topological property suggested by the extremely involved nature of the basin boundary structure of the bounded and unbounded attractors, which is the so-called Wada property. A boundary point is said to possess the Wada property if a hyper-sphere of any radius, centered at this point, contains pieces of all basins. A boundary itself possesses the Wada property when all its points have this property [25,26]. As a consequence, any boundary point is arbitrarily close to points of all basins of attraction [37]. Since one initial condition is always known within some small non-zero uncertainty, the uncertainty sphere will contains points of all basins, such that one has no previous certainty (whenever small the uncertainty radius may be) about to which basin will the trajectory asymptote to. As we have discussed in the previous section, a basin boundary with the Wada property has a vanishing uncertainty exponent α.

An example of Wada boundary in the wave interaction is depicted in Fig. 9(a), where we painted the basins of attraction using the same grayscale as in Fig. 3. Fig. 9(b) and (c) represent two successive magnifications of small boxes containing points of the three basins. They suggest that the basins possess the Wada property since they are intermixed in finer scales, in such a way that a boundary point is arbitrarily close to points of the three basins.

Let p be an unstable periodic orbit belonging to the boundary separating the basins of the attractors (bounded and unbounded). In order that the basin boundary possesses the Wada property, at least one of the complementary conditions below has to be satisfied [25,37]: (i) the stable manifold of the point p must be dense in the boundary of the three

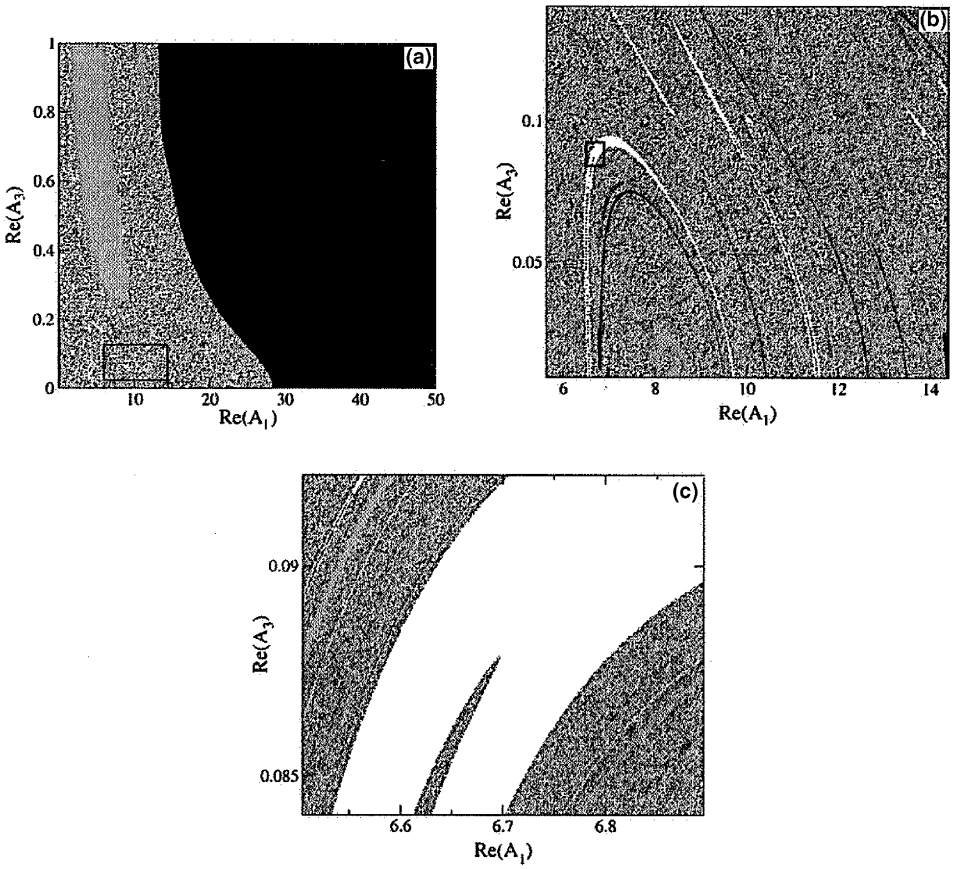

Fig. 9. (a) Re(A_1)–Re(A_3) projection of the phase space of the four-wave interaction system with $\Delta = 0.01$, $r = 1.0$, and showing the basins of attraction of the bounded attractors $P1$ (gray), $P3$ (white) and the infinity (black), (b) and (c): magnifications of small boxes (with black frames) as indicated.

basins; (ii) the periodic orbit p must be the only accessible orbit from one of the basins, denoted as $\mathscr{B}$. Otherwise, every unstable manifold of other periodic orbits that are accessible from $\mathscr{B}$ must intersect all basins. We say a boundary point p is accessible from a particular basin if there is another point in the interior of the basin which can be connected to p by a finite length curve that contains no boundary points except p [27]; (iii) the periodic orbit p must generate a basin cell. A cell is a region with a piecewise smooth boundary, whose edges are alternately pieces of stable and unstable manifolds of a periodic orbit. A basin cell is a cell that is a trapping region [26].

The direct numerical verification of these complementary conditions is rather difficult, so that we used another method to evidence the Wada property for the basin boundary in our problem. It consists on verifying that every open neighborhood of a boundary point intersects all basins [30]. This is equivalent to the previous conditions by using the following argument, where we use the fact that the Poincaré map $\mathbf{f}$ of the phase-space trajectories in the four-wave problem is invertible. Let us take a point p on the basin boundary, which is actually the stable manifold of p itself or some periodic orbit containing the point p. We take a small hyper-sphere $\mathscr{D}$ of initial conditions centered at p, and compute its forward images under the Poincaré map, $\mathbf{f}^m(\mathscr{D})$. As m increases, the image of $\mathscr{D}$ is a convoluted and very thin ribbon extending along the unstable manifold of p, as it is schematically shown in Fig. 10(a).

We have observed such a behavior, an example being shown in Fig. 10(b), where we have depicted images of a small ball of initial conditions (1) presumably intersecting the stable manifold of the saddle fixed point at the origin. The ellipse 2 is not, rigorously speaking, the image of the ball 1 under the flow generated by the vector field, but rather the image of the interior region of 1 which diverges the most, after a convenient number of iterations, and so on. These measures were taken to warrant adequate visualization of results. We see that the successive images 3, 4, etc. become extremely thin spaghetti-like filaments which tend to elongate along the direction of the unstable manifold corresponding to the origin saddle point.

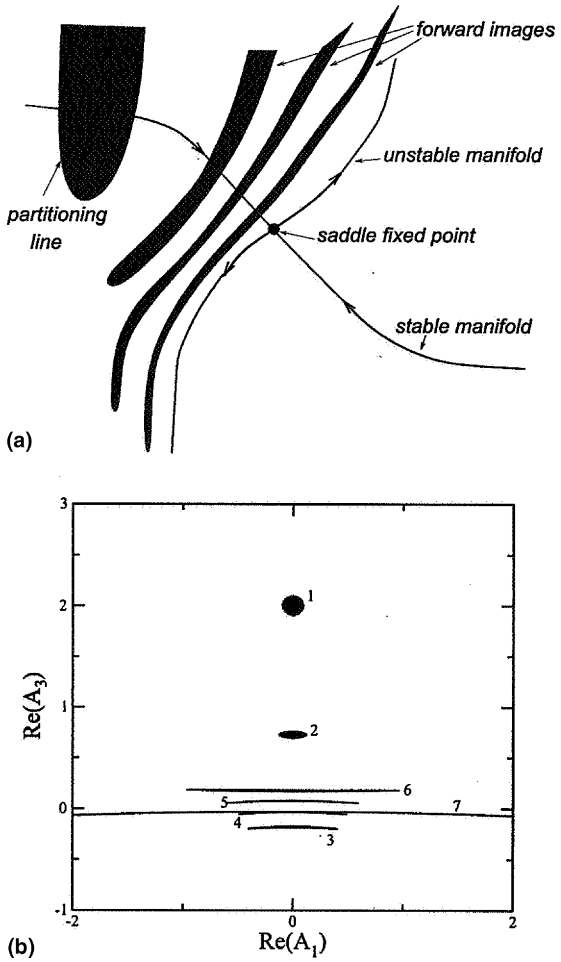

Fig. 10. (a) Scheme showing the formation of the incursive fingers of the basin boundary, (b) Actual behavior of a ball of initial conditions intercepting a stable manifold of the saddle point at the origin of the wave-interaction phase space, for $\Delta = 10^{-2}$ and $v = 0.8$.

The ball $\mathscr{D}$ is a connected set, and so are its images under the Poincaré map $\mathbf{f}$. Consider now that there is a finite value of $m = m_0$ such that $\mathbf{f}^{m_0}(\mathscr{D})$ intersects all the exit basins. Because $\mathbf{f}^{m_0}(\mathscr{D})$ maps to $\mathscr{D}$ under m_0 backward iterations, all the basin structures present in $\mathbf{f}^{m_0}(\mathscr{D})$ are also mapped into $\mathscr{D}$. Since we did not make any particular assumption about the radius of $\mathscr{D}$, and since the point p can be anywhere on the stable manifold, this statement is valid for any radius (whenever small), such that the entire stable manifold is a Wada basin boundary.

We have performed a statistical verification of the above claim by taking, in a phase space projection, a large number of small balls of radius ϵ, most of them crossing representative portions of the three basins [Fig. 11]. The centers of these ϵ-balls were randomly chosen. For the computation of $F(\epsilon)$ we did not discard any ϵ-ball center; but, in order to compute the fraction P in Fig. 12(a), we ignore those ϵ-balls that do not cross more than one basin. In other words, once a ϵ-ball has points converging to two attractors, we compute the fraction of them which also contain points belonging to third basin of attraction. In Fig. 12(a) we plot the fraction of ϵ-balls which contain points belonging to the three basins in Fig. 11, according to the previous criterion. We used the following procedure: for each uncertain point we have taken 500 nearby initial conditions and computed the fraction of cases presenting at least three different results for the final state. There have been used out of 16,000 points for each value of ϵ.

We see that, for a wide range of values of ϵ, all ϵ-balls (no fluctuations observed) contain points of the three basins. Hence, the centers of these balls are good numerical approximations of points belonging to a Wada boundary. In order to emphasize the connection between extreme final sensitivity and the presence of a Wada boundary we plot, in

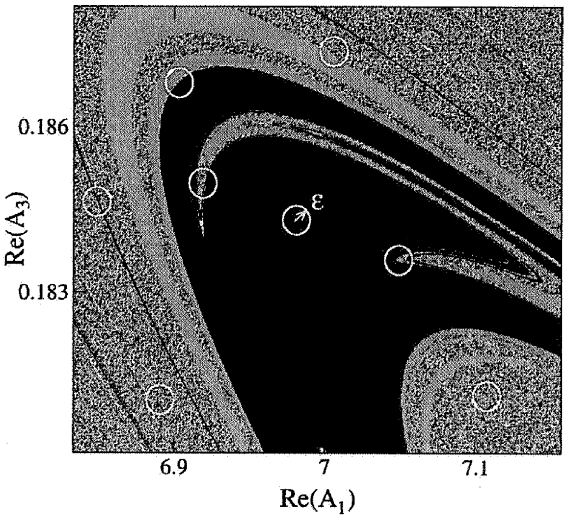

Fig. 11. A Re(A_1)–Re(A_3) projection of the phase space of the four-wave interaction system with $\Delta = 0.01$, $r = 1.0$, and showing the basins of attraction of the bounded attractors $P1$ (gray), $P3$ (white) and the infinity (black). We depict some of the ϵ-balls used to compute the uncertain fraction.

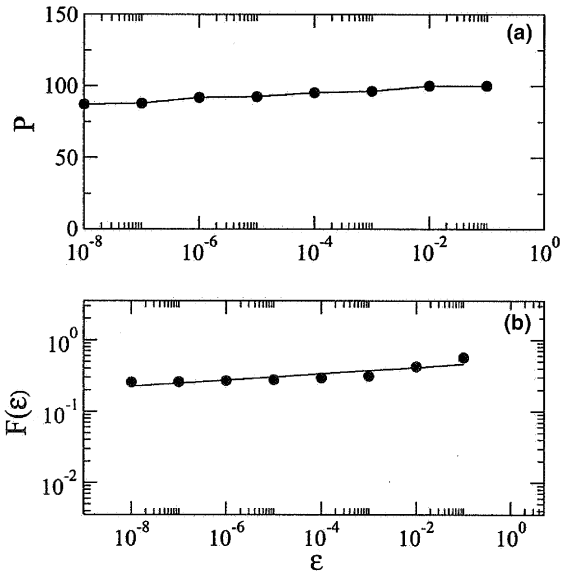

Fig. 12. (a) Percentile fraction of ϵ-balls, chosen in the basin boundary of the phase space projection of Fig. 11 ($\Delta = 0.01$), which contain points belonging to the three basins of attraction, (b) uncertain fraction of initial conditions versus uncertainty radius ϵ.

Fig. 12(b), the scaling of the ϵ-uncertain fraction of points, with a power-law fit with an uncertainty exponent ($\alpha = 0.04397 \pm 0.00961$) very close to zero, as required. It must be noted that, for obtaining this figure, we have taken a different region with respect to Fig. 4.

The robustness of this result lies in the fact that the above observations are barely affected by the value of the symmetry-breaking parameter. In Fig. 13 we perform the same kind of numerical testing as in Fig. 12, but for a value of Δ one order of magnitude higher. The results are basically the same, i.e. all boundary points have neighborhoods intercepting points of the three basins, for a wide range of radii, and a near-zero value of the uncertainty exponent ($\alpha = 0.01247 \pm 0.00132$).

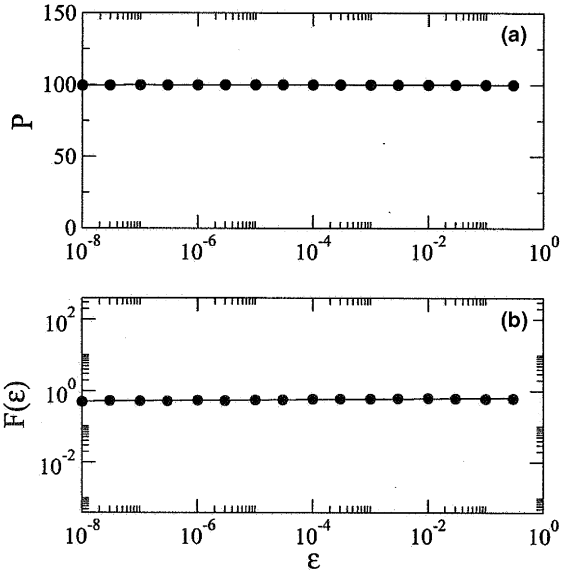

Fig. 13. (a) Percentile fraction of ϵ-balls which contain points belonging to the three basins of attraction for $\Delta = 0.1$. (b) Uncertain fraction of initial conditions versus uncertainty radius ϵ.

6. Conclusions

The parametric four-wave interaction problem is a non-integrable Hamiltonian system (for non-zero symmetry-breaking parameter), which turns itself into a high-dimensional dissipative system when we include damping and injection terms in the coupled-mode differential equation. The rich dynamical structure of the conservative dynamics translates into an equally complex behavior for the dissipative case. Far from exhausting the dynamical possibilities created by coexistent periodic and chaotic attractors, we limited ourselves to a parameter range where there are two coexistent bounded attractors and the attractor at infinity. Already in this case the basin structure is very complicated. We presented in this paper numerical evidence that the basins of the above-mentioned attractors are extremely interwoven. The basin boundary structure is so densely mixed that there is no way to answer, with total certainty, to which attractor the system asymptotes to, given an initial condition known up to some small error.

Final-state sensitivity is a universal feature of basin boundaries with a fractal geometry, but in the case we have analyzed in this paper the sensitivity is so high that the basin boundaries seems to present the Wada property. Wada-like basins, such as the interwoven basins of bounded and unbounded attractors, are so densely mixed that a point placed in the common boundary is arbitrarily close to all basins. This is clearly a non-trivial property, since in Euclidean sets such points would occur but isolately, whereas in Wada basins all boundary points have this property.

Acknowledgements

This work was made possible through partial financial support from the following Brazilian research agencies: CNPq and CAPES.

References

[1] Wersinger JM, Finn JM, Ott E. Phys Rev Lett 1980;44:453.
[2] Wersinger JM, Finn JM, Ott E. Phys Fluids 1980;23:1142.
[3] Kruer WL. The physics of laser plasma interactions. Redwood City, CA: Addison-Wesley; 1988.
[4] Chian AC-L, Lopes SR, Alves MV. Astron Astrophys 1994;290:L13.
[5] Chian AC-L, Rizzato FB. J Plas Phys 1994;51:61.
[6] Shen YR. The principles of nonlinear optics. New York: Wiley; 1984.

[7] Fischer P, Wiersma DS, Righini R, Champagne B, Buckingham AD. Phys Rev Lett 2000;85:4253.
[8] Rundquist A, Durfee III CG, Chang Z, Herne C, Backus S, Murnane MM, et al. Science 1998;280:1412.
[9] Spillane SM, Kippenberg TJ, Vahala KJ. Nature 2002;415:621.
[10] Deng L, Hagley EW, Wen J, Trippenbach M, Band Y, Julienne PS, et al. Nature 1999;398:218.
[11] Picozzi A, Haelterman M. Phys Rev Lett 2001;86:2010.
[12] Picozzi A, Haelterman M. Phys Rev Lett 2002;88:083901.
[13] Romeiras FJ. Phys Lett A 1983;93:227.
[14] Chian AC-L, Lopes SR, Abalde JR. Physica D 1996;99:169.
[15] Pakter R, Lopes SR, Viana RL. Physica D 1997;110:277.
[16] Coninck JCP, Lopes SR, Viana RL. Phys Rev E 2004;70:1.
[17] Feudel U, Witt A, Lai Y-C, Grebogi C. Phys Rev E 1998;58:3060.
[18] Coninck JCP, Lopes SR, Viana RL. Physica A 2004;343:247.
[19] Grebogi C, Kostelich E, Ott E, Yorke JA. Physica D 1987;25:347.
[20] Alexander JC, Yorke JA, You Z, Kan I. Int J Bifurcat Chaos 1992;2:795;
Sommerer JC, Ott E. Nature 1993;365:138;
Ott E, Sommerer JC, Alexander JC, Kan I, Yorke JA. Phys Rev Lett 1993;71:4134.
[21] Lai Y-C, Winslow RL. Physica D 1994;74:353.
[22] Blazejczyk-Okolewska B, Brindley J, Kapitaniak T. Chaos, Solitons & Fractals 2000;11:2511;
Yanchuk S, Kapitaniak T. Phys Rev E 2003;68:017202.
[23] Grebogi C, McDonald SW, Ott E, Yorke JA. Phys Lett A 1983;99:415.
[24] McDonald SW, Grebogi C, Ott E, Yorke JA. Physica D 1985;17:125.
[25] Nusse HE, Yorke JA. Science 1996;271:1376.
[26] Nusse HE, Yorke JA. Physica D 1996;90:242.
[27] Poon L, Campos J, Ott E, Grebogi C. Int J Bifurcat Chaos 1996;6:251.
[28] Aguirre J, Vallejo JC, Sanjuan MAF. Phys Rev E 2001;64:066208.
[29] Sweet D, Ott E, Yorke JA. Nature 1999;399:315.
[30] Toroczkai Z, Károlyi G, Péntek A, Tél T, Grebogi C, Yorke JA. Physica A 1997;239:235.
[31] da Silva EC, Caldas IL, Viana RL, Sanjuan MAF. Phys Plas 2002;9:4917.
[32] Sugihara R. Phys Fluids 1968;11:178.
[33] Karplyuk KS, Oraevskii VN, Pavlenko VP. J Plasma Phys 1973;15:113.
[34] Stenflo L. J Plas Phys 1970;4:585;
Chian ACL, Lopes SR, Alves MV. Astron Astrophys 1994;290:L13.
[35] Remmert R. Theory of complex functions. Berlin–Heidelberg–New York: Springer-Verlag; 1991.
[36] Eschenazi E, Solari HG, Gilmore R. Phys Rev A 1989;39:2609.
[37] Kennedy J, Yorke JA. Physica D 1991;51:213.